Kinesin-14 motors participate in a force balance at microtubule plus-ends to regulate dynamic instability

Allison Ogren[a], Sneha Parmar[a], Soumya Mukherjee[a], Samuel J. Gonzalez[a], Melissa Plooster[a], Mark McClellan[a], Anirudh G. Mannava[a], Elliott Davidson[b], Trisha N. Davis[b], and Melissa K. Gardner[a,1]

[a]Department of Genetics, Cell Biology, and Development, University of Minnesota, Minneapolis, MN 55455; and [b]Department of Biochemistry, University of Washington, Seattle, WA 98195

Edited by E. Ostap, Pennsylvania Muscle Institute, Raymond and Ruth Perelman School of Medicine at the University of Pennsylvania, Philadelphia, PA; received April 29, 2021; accepted January 3, 2022 by Editorial Board Member Yale E. Goldman

Kinesin-14 molecular motors represent an essential class of proteins that bind microtubules and walk toward their minus-ends. Previous studies have described important roles for Kinesin-14 motors at microtubule minus-ends, but their role in regulating plus-end dynamics remains controversial. Kinesin-14 motors have been shown to bind the EB family of microtubule plus-end binding proteins, suggesting that these minus-end–directed motors could interact with growing microtubule plus-ends. In this work, we explored the role of minus-end–directed Kinesin-14 motor forces in controlling plus-end microtubule dynamics. In cells, a Kinesin-14 mutant with reduced affinity to EB proteins led to increased microtubule lengths. Cell-free biophysical microscopy assays were performed using Kinesin-14 motors and an EB family marker of growing microtubule plus-ends, Mal3, which revealed that when Kinesin-14 motors bound to Mal3 at growing microtubule plus-ends, the motors subsequently walked toward the minus-end, and Mal3 was pulled away from the growing microtubule tip. Strikingly, these interactions resulted in an approximately twofold decrease in the expected postinteraction microtubule lifetime. Furthermore, generic minus-end–directed tension forces, generated by tethering growing plus-ends to the coverslip using λ-DNA, led to an approximately sevenfold decrease in the expected postinteraction microtubule growth length. In contrast, the inhibition of Kinesin-14 minus-end–directed motility led to extended tip interactions and to an increase in the expected postinteraction microtubule lifetime, indicating that plus-ends were stabilized by nonmotile Kinesin-14 motors. Together, we find that Kinesin-14 motors participate in a force balance at microtubule plus-ends to regulate microtubule lengths in cells.

kinesin | motor | microtubule | tubulin | dynamics

Microtubules are tubular filaments that represent a crucial component of the cellular cytoskeleton. Microtubules contribute to the cell's ability to change shape and size throughout its lifespan and play a fundamental role in cell division by establishing a mitotic spindle. Dynamic microtubule length changes are essential to the many functions of microtubules in cell growth, division, and differentiation (1). Microtubules undergo alternating periods of growth and shortening known as dynamic instability. This behavior is important for microtubule function in the cell, as it allows for rapid restructuring of the microtubule cytoskeleton (2). Here, microtubules tend to grow for an extended period of time and then suddenly and stochastically switch to a rapid shortening state (3). This switch from slow growth to rapid shortening, while critical for the ability of cells to rapidly restructure their microtubule cytoskeleton, is termed "catastrophe."

Dynamic instability can be controlled by forces generated from the microtubules themselves. For example, a large, force-dependent increase in the frequency of catastrophe events is observed when microtubules polymerize against a microfabricated barrier (4), which could occur when growing microtubules contact intracellular obstructions or a cell cortex. In contrast, microtubule shortening is stalled when microtubule plus-ends are captured by cortex-tethered dynein, leading to a pulling force in the direction of growth (5). Similarly, pulling on the microtubule plus-end in the direction of growth via an external force has been shown to contribute to elongation of the microtubules at the plus-ends (6). This type of tension-based pulling may occur in the context of a mitotic spindle, in which dynamic microtubule tips are tethered to chromosomes via a multiprotein kinetochore complex (7, 8).

Kinesin-14 motors comprise a family of kinesin motor proteins that generate ATP-dependent forces to walk along microtubules in the minus-end direction (9). Kinesin-14 motors are highly conserved in form and function across species, and in this study, we have focused on the Kinesin-14 of budding yeast (Kar3 with its binding partner Cik1) and human (HSET) for our experiments. Kinesin-14 motors contain a secondary diffusive microtubule interaction site at the N terminus that allows for the cross-linking and sliding of nearby microtubules (10). Thus, Kinesin-14 motors have important roles in the interaction between adjacent antiparallel microtubules, such as during

Significance

Kinesin-14 motors represent an essential class of molecular motors that bind to microtubules and then walk toward the microtubule minus-end. However, whether these motors can interact with growing plus-ends of microtubules to impact the lengthening of microtubules remains unknown. We found that Kinesin-14 motors could bind to a protein that resides at growing microtubule plus-ends and then pull this protein away from the growing end. This interaction acted to disrupt microtubule growth and decrease microtubule lengths in cells, likely by exerting minus-end–directed forces at the microtubule tip to alter the configuration of the growing microtubule plus-end. This work demonstrates general principles for the diverse roles that force-generating molecular motors can play in regulating cellular processes.

Author contributions: A.O. and M.K.G. designed research; A.O., S.P., S.M., S.J.G., M.P., and A.G.M. performed research; M.M., E.D., and T.N.D. contributed new reagents/analytic tools; A.O., S.P., S.M., S.J.G., M.P., A.G.M., and M.K.G. analyzed data; and A.O. and M.K.G. wrote the paper.

The authors declare no competing interest.

This article is a PNAS Direct Submission. E.O. is a guest editor invited by the Editorial Board.

[1]To whom correspondence may be addressed. Email: klei0091@umn.edu.

This article contains supporting information online at http://www.pnas.org/lookup/suppl/doi:10.1073/pnas.2108046119/-/DCSupplemental

Published February 16, 2022.

mitotic spindle assembly (11–13), and for the organization of microtubule minus-ends into spindle poles (14–19).

Recently, it has been shown that Kinesin-14 molecules are able to move rapidly and processively along microtubules. For yeast Kar3/Cik1 Kinesin-14 motors, it has been shown that single Kar3/Cik1 molecules are sufficient for processive movement on microtubules (11, 20). However, in contrast, recent work with HSET demonstrated that clusters of HSET molecules induce rapid, processive movement along microtubules (18, 21).

A recent in vitro study found that Kinesin-14 motors act to stabilize the microtubule minus-end by suppressing the tubulin off rate (19). However, experiments in cells suggest that Kinesin-14 motors could destabilize microtubules, potentially at their growing microtubule plus-ends (22, 23). Thus, whether Kinesin-14 motors could differentially alter the stability of microtubule plus-ends and minus-ends remains an open question. In this study, we sought to investigate the effects of a minus-end directed motor on the stability of a growing microtubule plus-end.

How could a minus-end–directed Kinesin-14 motor interact with a growing microtubule plus-end? Importantly, Kinesin-14 motors contain domain(s) that allow for direct binding to plus-end tip trackers such as EB1 (human) and Mal3 (yeast) (24–27). Thus, we hypothesized that, even under conditions in which Kinesin-14 motors can move robustly toward microtubule minus-ends, the binding of Kinesin-14 motors to a plus-end tip tracker such as Mal3 could allow for interactions with the growing microtubule plus-end. These interactions could then exert a minus-end–directed force on the tip tracker, and on the plus-end tip itself, as the motor moves toward the minus-end. Thus, by exerting minus-end–directed pulling forces, Kinesin-14 motors could potentially destabilize the growing microtubule plus-end. Recent work found that the EB1–Kinesin-14 complex contributes to the proper organization of the metaphase mitotic spindle (25) and that EB1 and Kinesin-14 complexes work together to guide growth of parallel microtubules from a common nucleating center (26). However, the effect of minus-end–directed forces in regulating the dynamics of growing microtubule plus-ends has not been explored.

In this study, we found that, after a plus-end interaction, minus-end–directed Kinesin-14 motors pulled Mal3 from a growing microtubule end, thus increasing the likelihood of a catastrophe event. Similarly, generic minus-end–directed tension forces led to catastrophe at growing microtubule plus-ends. In contrast, the inhibition of minus-end–directed Kinesin-14 motility led to extended tip interactions and the suppression of catastrophe. Together, our work indicates that Kinesin-14 motors cooperate with microtubule tip tracking proteins to limit microtubule lengths by exerting minus-end–directed forces at growing microtubule plus-ends.

Results

Yeast Kinesin-14 Briefly Binds to the Plus-Ends of Growing Microtubules in the Presence of Mal3. To examine the interaction of Kinesin-14 motors with growing microtubule plus-ends, we first purified the Kinesin-14 motor protein Kar3-GFP/Cik1 directly from log-phase yeast cells (11). Furthermore, as a negative control, a four-amino-acid mutant of Cik1 containing a string of four alanine residues in the SxIP EB binding domain was generated (Cik1-4A), and then the Kar3-GFP/Cik1-4A mutant protein was also purified directly from mutant log-phase yeast cells. We expected that the Kar3-GFP/Cik1-4A mutant protein complex would be less likely to interact with growing microtubule plus-ends because of disruption in its EB binding domain.

To directly probe the interaction between Kinesin-14 motor proteins and the growing plus-ends of dynamic microtubules, cell-free biophysical microscopy assays were used. Here, Alexa-647–labeled microtubules were grown from seed templates (Fig. 1 *A*, *Top*, blue) in the presence of the fission yeast EB protein Mal3-mCherry (28) (Fig. 1 *A*, *Top*, magenta). Furthermore, either wild-type Kar3-GFP/Cik1 or mutant Kar3-GFP/Cik1-4A (Fig. 1 *A*, *Top*, green) was introduced into flow chambers containing the dynamic microtubules and Mal3-mCherry. The interaction of the Kinesin-14 motors with the dynamic plus-ends of the growing microtubules was then observed using total internal reflection fluorescence (TIRF) microscopy. We observed the Kar3/Cik1 protein complex briefly interacting with growing microtubule plus-ends (Fig. 1 *A*, *Bottom Left*, white arrows), which was less frequently observed in experiments with the Kar3/Cik1-4A protein complexes (Fig. 1 *A*, *Bottom Right*; similar to in yeast cells, *SI Appendix*, Fig. S1*A*).

Kymographs were then constructed, and "tip events" were defined as interactions in which a Kinesin-14 motor occupied the same pixel coordinates as the dynamic plus-end tip for at least one imaging frame (Fig. 1 *A*, *Bottom*, white arrows; blue diamonds: non-tip lattice interactions). We calculated the fraction of dynamic plus-end growth cycles in which a tip event occurred in the presence of the wild-type and the Cik1-4A mutant proteins and found that the fraction of microtubules with tip events was ∼2.7-fold higher with wild-type motors than for the Cik1-4A motors (Fig. 1*B*, $P < 0.00001$, Z statistic = 4.963). We note that, overall, the targeting of Kar3-GFP/Cik1-4A to the dynamic microtubule lattice appears to be reduced as well, likely because residual Mal3 along the microtubule length aides in targeting wild-type Kar3–Cik1 to the dynamic microtubule lattice. We conclude that the interaction of Kar3/Cik1 with growing microtubule plus-ends is facilitated by Kinesin-14 binding to the EB protein Mal3.

Interaction of Kinesin-14 Motors with Growing Microtubule Plus-Ends Restricts Microtubule Lengths in Cells. We then asked whether the interaction of Kinesin-14 motors with dynamic microtubule plus-ends could alter microtubule lengths in cells. Because the Cik1-4A mutation disrupts the interaction of Kinesin-14 motors with growing microtubule plus-ends (Fig. 1*B*), we compared microtubule lengths in wild-type cells and in cells that expressed the Cik1-4A mutation.

First, we examined the effect of the Cik1-4A mutant within the anaphase mitotic spindle. Specifically, we used a cell line that expressed the Kinesin-5 motor Kip1–GFP along with fluorescent spindle pole markers, and by collecting late anaphase spindle images, we measured the "midzone" length, which is the length of overlap between antiparallel interpolar microtubules, visible via the microtubule cross-linking Kip1–GFP motors (Fig. 1 *C* and *D* [orange box, midzone]). The late anaphase "midzone length" reflects the length of interpolar microtubules within the anaphase mitotic spindle such that a longer midzone length reflects an increase in interpolar microtubule lengths. We quantified late anaphase midzone length using semiautomated MATLAB code to measure the length of the bright microtubule overlap zone at the center of late anaphase spindles (Fig. 1 *C* and *D*, orange boxes; *Materials and Methods*). We found that the Cik1-4A cells had an ∼24% increase in late anaphase midzone length relative to wild-type cells (Fig. 1*E*, $P < 0.0001$, Student's t test), indicating that the interaction of Kar3/Cik1 with growing microtubule plus-ends acted to shorten interpolar microtubules during anaphase. Consistent with previous reports (29–34), we found that the increased midzone lengths in the Cik1-4A cells also drove a concomitant increase in pole-to-pole spindle lengths (*SI Appendix*, Fig. S1 *B* and *C*).

Second, we used a tubulin-GFP–expressing yeast cell line to examine the effect of the Cik1-4A mutation on individual

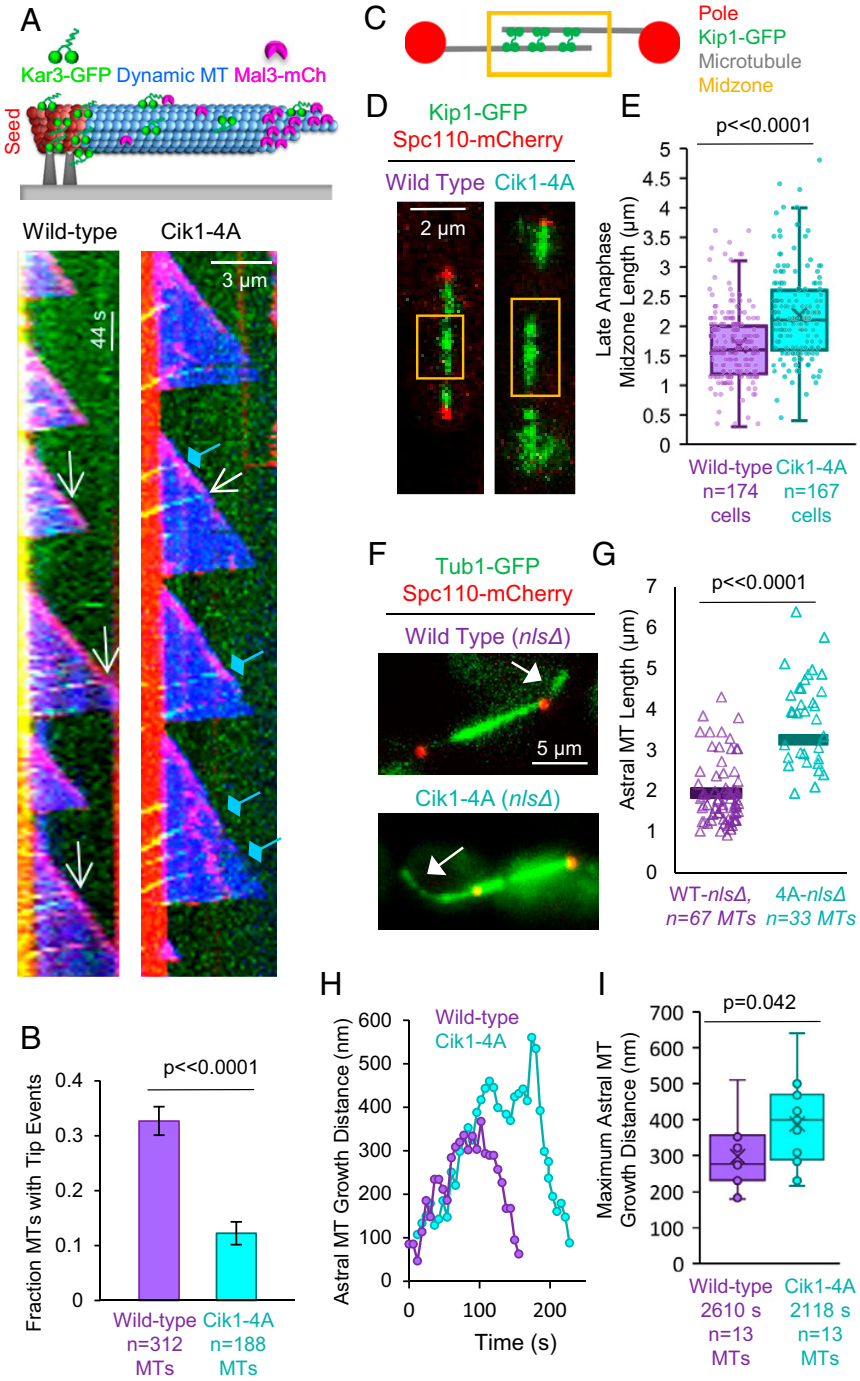

Fig. 1. Kinesin-14 motors interact with EB proteins at microtubule plus-ends and suppress the length of microtubules in cells (*A*, *Top*) Cell-free assays: microtubule seeds (dark red) with dynamic microtubule extensions (blue). Kar3-GFP/Cik1 (green) allowed for the visualization of Kinesin-14 binding to microtubules, and Mal3-mCherry (magenta) is an EB tip protein. (*Bottom*) Kar3-GFP/Cik1 (yeast Kinesin-14) interacts with growing microtubule plus-ends (*Left*, white arrows). A Cik1-4A mutant has a mutated Mal3 binding domain and more rarely interacts with growing microtubule plus-ends (*Right*: blue diamonds: non-tip lattice interactions). (*B*) The proportion of microtubules with tip interaction events for wild-type and Cik1-4A mutant protein ($P < 0.0001$, Z-test). (*C*) Schematic of late anaphase yeast mitotic spindle. Orange box indicates the interpolar microtubule overlap zone called the "midzone." (*D*) Late anaphase midzone length was measured in yeast cells using a semiautomated MATLAB code (orange boxes). (*E*) The midzone length is longer in Cik1-4A mutant cells relative to wild-type cells ($P < 0.0001$, Student's *t* test). On each box, the central line indicates the median, the bottom and top edges of the box indicate the 25th and 75th percentiles, and the marker within the box indicates mean. (*F*) Cytoplasmic astral microtubule length was measured in yeast cells with the Kar1 and Cik1 nuclear localization signals (*nls*) deleted. The white arrow indicates an individual astral microtubule. (*G*) The cytoplasmic astral microtubule length is longer in Cik1-4A mutant cells relative to wild-type cells ($P < 0.0001$, Student's *t* test). (*H*) Cytoplasmic astral microtubule growth trace in wild-type (purple) and Cik1-4A (cyan) cells. (*I*) Maximum cytoplasmic astral microtubule growth length. On each box, the central line indicates the median, the bottom and top edges of the box indicate the 25th and 75th percentiles, and the marker within the box indicates mean.

cytoplasmic astral microtubules in yeast cells (Fig. 1*F*, white arrows). Because yeast undergoes a closed mitosis and Kar3/Cik1 is transported into the nucleus for cell division, we generated strains with the Kar3/Cik1 nuclear localization signal knocked out (*nls*Δ; *Materials and Methods*). Thus, the *nls*Δ strains allowed us to visualize how alterations to the interaction

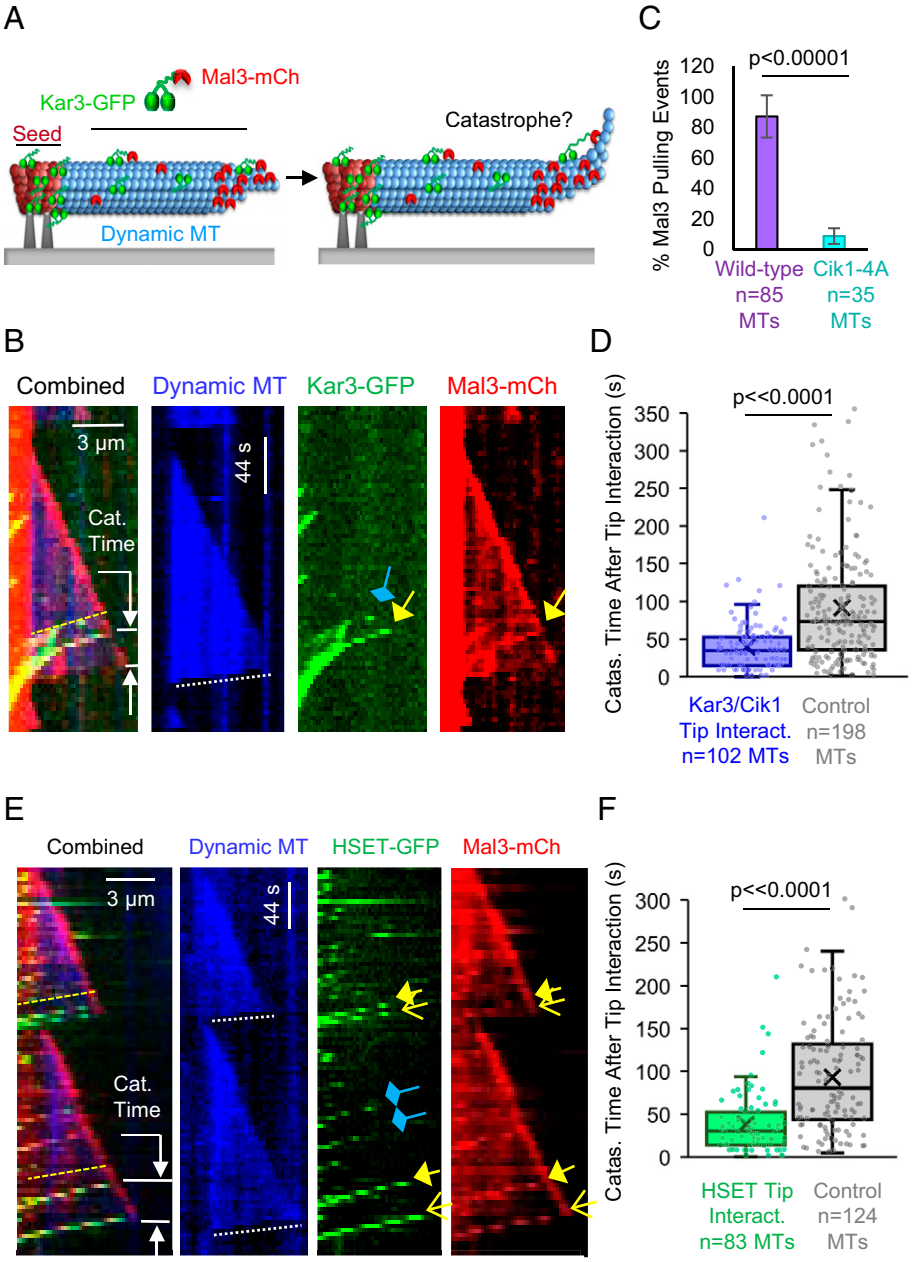

Fig. 2. Kinesin-14 motors pull EB proteins from growing microtubule tips, causing premature catastrophe. (*A*) Hypothesis for interaction of Kinesin-14 motors with EB proteins at growing microtubule plus-ends: Kar3/Cik1 binds to the EB tip tracker, and when the Kinesin-14 motor walks toward the minus-end, it exerts minus-end–directed forces to pull back on the EB tip tracker, thus disrupting the plus-end structure and destabilizing the plus-end, causing catastrophe. (*B*) Mal3 (red) is pulled away from the tip by Kar3/Cik1 (green) just prior to catastrophe (yellow arrows and yellow dashed lines; Movie S1). Walking events in which the (green) Kinesin-14 motor did not interact within the same pixel as the microtubule plus-end tip were excluded from the analysis (blue diamonds). The time to catastrophe after Kar3/Cik1 tip interaction was measured (white arrows). (*C*) The percentage of Kinesin-14 microtubule plus-end tip interactions that led to Mal3 being pulled away from the growing microtubule plus-end. (Movie S2). (*D*) Catastrophe events occurred ~2.3-fold more quickly after a Kar3/Cik1 tip interaction than was predicted for a control tip interaction (*SI Appendix*, Fig. S2*A*, $P < 0.0001$, K-S test). On each box, the central line indicates the median, the bottom and top edges of the box indicate the 25th and 75th percentiles, and the marker within the box indicates mean. (*E*) Mal3 (red) is pulled away from the tip by HSET (human Kinesin-14) just prior to catastrophe (yellow arrows and yellow dashed lines; open yellow arrows represent later interaction, not included in quantification of time to catastrophe after interaction; Movie S3). Walking events in which the (green) Kinesin-14 motor did not interact within the same pixel as the microtubule tip were excluded from the analysis (blue diamonds). The time to catastrophe after the HSET tip interaction was measured (white arrows). (*F*) Catastrophe events occurred ~2.5-fold more quickly after an HSET tip interaction than was predicted for a control tip interaction (*SI Appendix*, Fig. S2*B*, $P < 0.0001$, K-S test). On each box, the central line indicates the median, the bottom and top edges of the box indicate the 25th and 75th percentiles, and the marker within the box indicates mean.

of Kinesin-14 motors with growing microtubule plus-ends could change individual cytoplasmic astral microtubule lengths (Fig. 1*F*, white arrows). Fluorescence images of yeast cytoplasmic astral microtubules were collected, and the astral microtubule length was measured. We found that in cells expressing the mutant Cik1-4A protein, astral microtubules had a 91% increase in length relative to wild-type cells (Fig. 1*G*, $P < 0.0001$, Student's t test). Together, our results demonstrate that the interaction between Kinesin-14 motor proteins and growing microtubule plus-ends acts to restrict the length of microtubules in cells.

Finally, we collected movies of astral microtubule dynamics in wild-type and Cik1-4A cells. Here, we tracked growing and shortening plus-ends (Fig. 1*H*), and for each microtubule, we measured the longest growth displacement length that was observed prior to an extended shortening event. We found that microtubules in Cik1-4A mutant cells reached greater terminal lengths prior to a catastrophe event as compared to wild-type cells (Fig. 1*I*, $P = 0.042$). Thus, the interaction between Kinesin-14 motors and growing microtubule plus-ends restricts the length of microtubules in cells by limiting the distance that microtubules grow prior to a catastrophe event.

Pulling of EB Proteins from Growing Microtubule Tips by Kinesin-14 Motors Leads to Catastrophe Events. How could the interaction between Kinesin-14 motors and growing microtubule plus-ends limit the distance that microtubules grow prior to a catastrophe event? Given that Kinesin-14 motor proteins are minus-end directed and that Cik1 contains an EB binding domain (SxIP) at its extreme N terminus (25), we hypothesized that Cik1 could bind to Mal3 at the microtubule plus-end (Fig. 2 *A*, *Left*, red/green), and then Kinesin-14 motor(s) could pull EB tip tracker(s) from the growing microtubule plus-end as the motor(s) walked toward the microtubule minus-end, thus disrupting the configuration of the growing microtubule plus-end (Fig. 2 *A*, *Right*). This disruption could then destabilize the growing plus-end, leading to catastrophe (Fig. 2*A*).

To test this idea, we turned to cell-free reconstitution assays. Specifically, we used purified proteins and collected movies of Kar3-GFP/Cik1 motors interacting with Mal3-mCherry at growing microtubule plus-ends (Fig. 2*B*). While Kar3-GFP/Cik1 (Fig. 2*B*, green) frequently bound to the dynamic microtubule lattice (Fig. 2*B*, blue diamond), interactions with Mal3 at the growing microtubule plus-end were also observed (Fig. 2*B*, yellow arrow). Importantly, we observed that, when the Kar3/Cik1 motors interacted with Mal3 at the growing microtubule tip (instances in which the motor fluorescence occupied the same pixel as the microtubule tip fluorescence for at least one imaging frame), 87% of these tip interactions resulted in the minus-end–directed motors actively pulling Mal3 away from the plus-end tip (Fig. 2*B*, yellow dashed lines, and Fig. 2*C*, $n = 85$ total tip events; Movie S1). In contrast, we observed that, for the Kar3/Cik1-4A mutant motors with weakened affinity for Mal3, only 8.6% of the observed tip interactions resulted in the motors actively pulling Mal3 away from the plus-end tip (Fig. 2*C*, $n = 35$ total tip events, $P < 0.00001$, $Z = 6.97$; Movie S2).

Importantly, after Mal3 was pulled away from growing microtubule plus-ends by Kar3/Cik1 motors (Fig. 2*B*, yellow dashed lines and yellow arrows), microtubule catastrophe events frequently followed (Fig. 2*B*, white dotted line). To determine whether this type of Mal3 pulling event directly increased the likelihood of a microtubule catastrophe event, the time to catastrophe after a Kar3/Cik1 tip interaction was measured (Fig. 2 *B*, *Left*, white arrows). In this instance, a "tip interaction" was defined as instances in which the motor fluorescence occupied the same pixel as the microtubule tip fluorescence for at least one time step followed by the simultaneous movement of Kinesin-14 and Mal3 molecules away from the tip, regardless of whether the plus-end Mal3 signal intensity was changed after the interaction (Fig. 2 *B*, *Left*, yellow dashed lines). Walking events in which the (green) Kinesin-14 motor did not interact with the same pixel as the microtubule tip were excluded from the analysis (Fig. 2*B*, blue diamond). The time to catastrophe after a tip interaction was calculated by measuring the number of time frames between the initial motor-tip event and the catastrophe event and then by dividing this value by the frame rate (in seconds^{-1}) to find the time to catastrophe in seconds. If multiple tip interactions were observed prior to a catastrophe event, the number of time frames between the first tip interaction and the catastrophe event was used.

The time to catastrophe after a Kar3/Cik1 tip interaction was then compared to control events in which the total microtubule growth time prior to catastrophe ("catastrophe time") was measured for control microtubules that had no Kar3/Cik1 tip interaction, and then each of these catastrophe times was multiplied by a uniformly distributed random number between 0 and 1 to generate a theoretical "tip interaction" time point. The difference between this theoretical tip interaction time point and its associated experimental microtubule catastrophe time represented the values for the control dataset in each dynamic microtubule experiment.

We found that, after a Kar3/Cik1 tip interaction, microtubules underwent catastrophe ~2.3-fold more quickly than was predicted for the control tip interaction events (Fig. 2*D* and *SI Appendix*, Fig. S2*A*, $P < 0.0001$, K-S test). Thus, the interaction of Kar3/Cik1 with Mal3 at growing microtubule plus-ends, in which Kar3/Cik1 pulled Mal3 away from the tip, had a dramatic effect on destabilizing the growing plus-end, leading to catastrophe.

We then asked whether this behavior would be common to other Kinesin-14 molecular motors. Thus, we purified the human Kinesin-14 HSET–GFP (19) (*Materials and Methods*) and performed experiments using HSET–GFP. Similar to Kar3/Cik1 (Fig. 2*B*), HSET frequently bound to the dynamic microtubule lattice (Fig. 2*E*, blue diamonds), but interactions of HSET with Mal3 at the growing microtubule plus-end were also observed (Fig. 2*E*, yellow arrows). Similar to the Kar3–Cik1 analysis, HSET walking events in which the (green) Kinesin-14 motor did not interact with the same pixel as the microtubule tip were excluded from the analysis (Fig. 2*E*, blue diamonds). We found that HSET interacted with growing microtubule plus-ends at similar rates to Kar3/Cik1 (*SI Appendix*, Fig. S1*D*, $P = 0.896$, Z statistic $= -0.131$). In contrast, in the absence of Mal3, HSET rarely interacted with the growing microtubule tip (*SI Appendix*, Fig. S1 *E* and *F*, $P < 0.00001$, Z statistic $= 4.46$).

Importantly, we again observed that, when the HSET motors interacted with Mal3 at the growing microtubule tip, the motors pulled Mal3 away from the plus-end tip as they journeyed toward the minus-end (Fig. 2*E*, yellow dashed lines, and Movie S3). Similar to the Kar3/Cik1 experiments, we noted that this interaction appeared to be quickly followed by a catastrophe event (Fig. 2*E*, dotted white lines). We defined a "tip interaction" as an event in which Mal3 and the HSET motor(s) occupied the same pixel coordinates for at least one imaging frame and then moved simultaneously and together away from a growing microtubule plus-end (Fig. 2 *E*, *Left*, dashed yellow lines), regardless of the degree of Mal3 signal changes at the growing microtubule plus-end. We found that catastrophe events occurred ~2.5-fold more quickly after an HSET tip event than was predicted for a control tip interaction (Fig. 2*F* and *SI Appendix*, Fig. S2*B*, $P < 0.0001$, K-S test).

We note that, for both Kar3/Cik1 and HSET, we occasionally observed events in which a tip interaction event was followed by another tip interaction event before catastrophe (~23% of Kar3-Cik1 events, ~27% of HSET events), including events in

which the final tip interaction was coincident with the catastrophe itself. In order to conservatively characterize the effect of Kinesin-14 motors on the time to catastrophe, we selected the earliest tip interaction in our quantification of time to catastrophe after interaction.

Previous studies have shown that multiple HSET motors form a complex to drive processive HSET movement in vitro (18, 21). In contrast, studies have shown that single Kar3/Cik1 molecules drive processive minus-end–directed motor movement (11, 20). Thus, we compared the fluorescence intensity of moving Kar3-GFP/Cik1 and HSET–GFP motors (*SI Appendix*, Fig. S4 *A* and *B*). We found that the SD of fluorescence intensities for the HSET molecules was ∼64% larger than for the Kar3-GFP motors, suggesting that, consistent with previous observations, HSET may form multimotor complexes to enhance its processivity. Thus, multiple HSET motors could act as a complex to pull Mal3 away from growing microtubule tips, perhaps accumulating additional residual Mal3 that is associated with the lattice as the complex moves toward the minus-end.

To characterize Kinesin-14 motor movement along the dynamic microtubule lattice as well as at the growing microtubule tip, we measured Kinesin-14 motor walking velocities both on the guanoside diphosphate (GDP) lattice of the dynamic microtubule extensions as well as on the GMPCPP (GTP analog) seeds (*SI Appendix*, Fig. S4 *C–F*). We found that the HSET motors walked ∼39% more slowly on the GMPCPP seeds as compared to the GDP lattice (*SI Appendix*, Fig. S4 *C* and *D*), and the Kar3/Cik1 motors walked ∼63% more slowly (*SI Appendix*, Fig. S4 *E* and *F*). We speculate that the slowing of the Kinesin-14 motors on the GTP lattice could increase their duration time at growing microtubule ends, thus increasing the likelihood of interactions with tip-bound Mal3.

Taken together, these results show that, in general, the interaction of Kinesin-14 motors with EB proteins at growing plus-ends directly results in microtubule catastrophe events and that this is a conserved phenomenon between yeast and human Kinesin-14 motors.

Kinesin-14 Motors with Inhibited Motility Are Plus-End Tip Trackers That Stabilize Growing Plus-Ends. The observation that Kinesin-14 motors pulled EB proteins away from the growing microtubule tip (Fig. 2 *B* and *E*) suggests that the motors exert minus-end–directed forces to tug on protofilaments at the microtubule plus-end, thus disrupting growth and ultimately causing a catastrophe event (Fig. 2*A*). If this model is correct, we predicted that the inhibition of Kinesin-14 motility would eliminate this catastrophe effect because of the loss of minus-end–directed motor forces. Thus, we used AMP-PNP (adenylyl-imidodiphosphate), which is a slowly hydrolyzable analog of ATP, to inhibit Kinesin-14 mobility (35). We therefore performed experiments with ATP, AMP-PNP, and with an equal mixture of ATP and AMP-PNP.

In conditions with excess ATP (4 mM), we observed that HSET tip interactions were brief (Figs. 2*E* and 3*A*, white arrows). However, in mixed ATP/AMP-PNP (2 mM/2 mM) conditions, HSET tip interactions were more prolonged, with HSET tracking the growing microtubule plus-end during the tip interaction (Fig. 3*B*, white lines/arrows). Finally, in experiments with only AMP-PNP (4 mM), HSET tip interactions were much more prolonged, with HSET again tracking the growing microtubule plus-end during the tip interaction (Fig. 3*C*, *SI Appendix*, Fig. S2*D*, white lines/arrows, and Movie S4; similar results were observed in Kar3/Cik1, *SI Appendix*, Fig. S2*E*). In summary, we observed an ∼15-fold increase in the fraction of microtubule growth time in which HSET was present at the growing plus-end in AMP-PNP as compared to ATP conditions, with an approximately fivefold increase in mixed AMP-PNP/ATP conditions as compared to ATP conditions (Fig. 3*D*, $P < 0.0001$, ANOVA). Tip tracking of HSET in AMP-PNP suggests that the HSET motor is mobility inhibited but perhaps not strongly bound to the microtubule lattice. This behavior could be due to GTP competition with AMP-PNP or a reduced affinity of AMP-PNP to Kinesin-14 motor head domains (36, 37). Thus, a single HSET motor head or, alternatively, the second microtubule binding domain on the HSET N-terminal tail, could contribute to persistent binding to and diffusive-like transport of Kinesin-14 motors on the tips of growing microtubules (20).

We then asked whether the inhibition of HSET mobility would change HSET's effect on catastrophe events at the growing microtubule plus-end. Therefore, we measured the time to catastrophe after the start of an HSET tip interaction and compared the results for various nucleotide groups to the control tip interactions. In the presence of ATP, catastrophe events occurred more quickly after an HSET tip interaction event than for control interaction events in which a random interaction time was selected on microtubules with no HSET tip interaction (Fig. 3*E*, green). However, strikingly, HSET had the opposite effect on catastrophe when its mobility was suppressed: for the 100% AMP-PNP experiments, the catastrophe time after the start of a tip interaction was ∼88% longer than for the control interaction events and ∼355% longer than for HSET tip interactions in ATP (Fig. 3*E* and *SI Appendix*, Fig. S2*F*, red). There was a more moderate growth stabilization effect for the mixed ATP/AMP-PNP experiments (Fig. 3*E* and *SI Appendix*, Fig. S2*F*, orange; $P < 0.0001$, ANOVA). We note that the control catastrophe times were indistinguishable between all of the nucleotide conditions (*SI Appendix*, Fig. S2 *G* and *H*, $P = 0.673$, ANOVA), and so a combined control data set was used in Fig. 3*E* (gray).

Thus, under conditions in which Kinesin-14 mobility is inhibited, interactions of Kinesin-14 motor proteins with EB proteins at growing microtubule plus-ends acted to stabilize the plus-end against catastrophe, which is the opposite effect that we observed for Kinesin-14 motors in ATP (Fig. 3*E*). Taken together, these results indicate that Kinesin-14 participates in a regulatory force balance at the dynamic microtubule plus-end tip.

Computational Simulations: Disruption of a Single Protofilament for ∼10-s Results in Premature Catastrophe. Why do premature catastrophe events occur following the Kinesin-14 motor–mediated removal of EB protein(s) from the growing microtubule tip? One possible explanation could be that microtubule protofilament(s) are pulled back by motor/EB complexes, resulting in a curled configuration (Fig. 2 *A*, *Right*). The curling back of protofilament(s), similar to the configuration of a disassembling microtubule (38), could frustrate the addition of new tubulin subunits at the curled protofilament ends (39, 40), halting the protofilament growth.

To test this idea, we turned to computational simulations. Specifically, we adapted a previously described three-dimensional molecular-scale computational model for microtubule assembly to explore the sensitivity of catastrophe events to protofilament growth disruptions (41–43). This model explicitly considers the contribution of protofilaments to overall microtubule growth and catastrophe via lateral and longitudinal bonds between each tubulin subunit (41–43). In the simulation, each newly arriving tubulin subunit is stabilized within the growing microtubule lattice by bonding to the lateral neighbors on either side of it and by establishing a longitudinal bond with the tubulin subunit below it. Thus, if protofilaments are curled back, preventing them from growing coordinately with the remainder of the microtubule (Fig. 4*A*, step 2), some of the newly arriving tubulin subunits would be missing a lateral

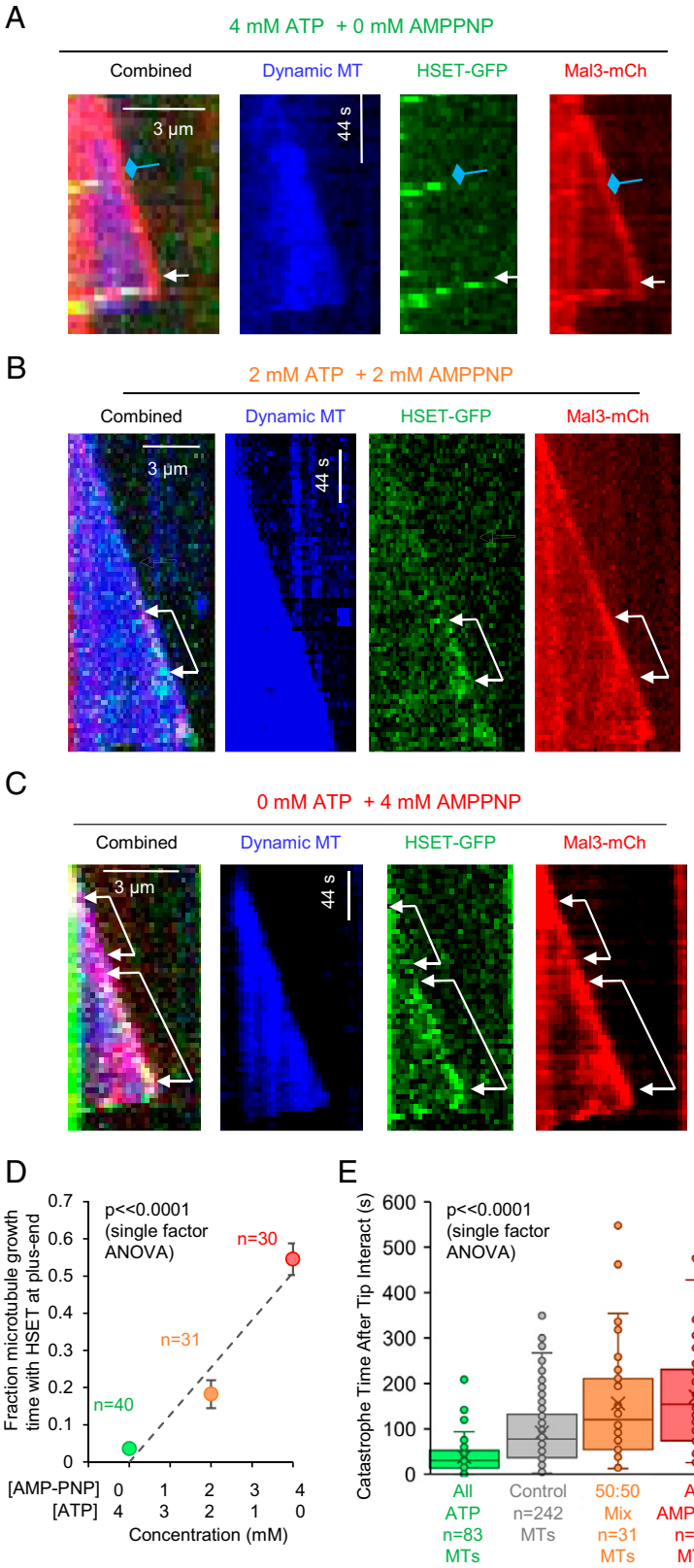

Fig. 3. Kinesin-14 motors with inhibited minus-end motor activity stabilize plus-end growth. (*A*) In 100% ATP conditions (4 mM), HSET tip interactions were brief and occurred just prior to catastrophe (white arrow; blue diamond represents non-tip interaction). (*B*) In a ratio of 50:50 mixed ATP/AMP-PNP conditions (2 mM/2 mM), HSET tip interactions were prolonged. (*C*) In 100% AMP-PNP conditions (4 mM), HSET tip interactions were severely prolonged, and interactions often occurred long before catastrophe (*SI Appendix*, Fig. S2*D* and Movie S4). (*D*) HSET interacts with the plus-end for longer period of time with inhibited Kinesin-14 mobility ($P < 0.0001$, ANOVA). (*E*) Catastrophe is delayed, and microtubule plus-end growth stabilized when HSET motor activity is suppressed (*SI Appendix*, Fig. S3*F*; $P < 0.0001$, ANOVA). On each box, the central line indicates the median, the bottom and top edges of the box indicate the 25th and 75th percentiles, and the marker within the box indicates mean.

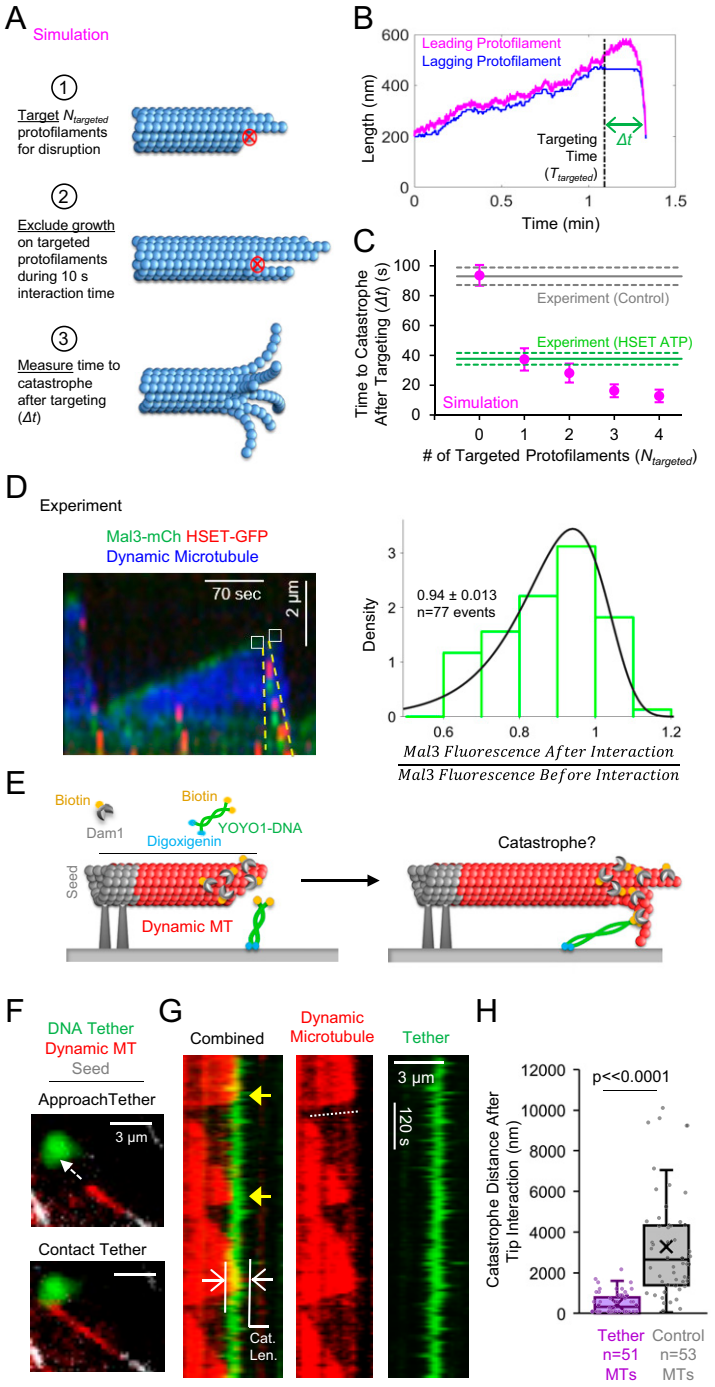

Fig. 4. In simulations and in generic tether pulling experiments, minus-end–directed forces that disrupt microtubule plus-ends lead to catastrophe events. (*A*) Simulation method: Step 1: identify the number of protofilament(s) to be targeted for growth disruption at the plus-end ($N_{targeted}$). Step 2: exclude growth on the targeted protofilament(s) at time $T_{targeted}$ for a duration of $D_{targeted}$. Step 3: measure the time to catastrophe after targeting (Δt). (*B*) A representative simulation trace for disruption of one protofilament (magenta: leading microtubule protofilament length; blue: lagging protofilament length). Green: Δt, the difference between the protofilament targeting time ($T_{targeted}$) and the catastrophe time. (*C*) The disruption of one to two microtubule protofilaments for ~10 s reproduces experimental catastrophe observations. (*D*, *Left*) Kymographs were generated to estimate Mal3 lost during an HSET tip interaction (white boxes). Events were classified as tip interactions if HSET was colocalized with the pixel at the microtubule tip for at least one time step, and then Mal3 and HSET traveled simultaneously away from the growing microtubule plus-end (yellow dashed lines). (*Right*) Fitting to the distribution of Mal3 fluorescence loss ratios after HSET plus-end tip interaction. (*E*) Schematic of DNA tethering experiments. YOYO1-labeled DNA is bound to the coverslip at one end and Dam1 at its opposite end. As microtubules grow, their plus-ends are "caught" by the DNA tether, and this pulls back on the plus-end. (*F*) DNA tethers are attached to coverslips (green), and microtubules occasionally interact with the tethers as they grow (white dashed line shows direction of microtubule growth prior to interaction (dynamic microtubule in red; Movie S5). Growth past DNA tether is measured from the start of interaction with the green tether in the direction of microtubule growth. (*G*) Kymographs resulting from DNA-tethering experiments. The DNA tether is shown in green, and dynamic microtubules are in red. Yellow arrows show occurrences of the growing plus-end being caught by a tether, resulting in catastrophe (dotted white line). White arrows: measurement of catastrophe distance after interaction with tether. (*H*) Castastrophe distance after a tether interaction as compared to a control tip interaction (*SI Appendix*, Fig. S3*D*, $P < 0.0001$, K-S test). On each box, the central line indicates the median, the bottom and top edges of the box indicate the 25th and 75th percentiles, and the marker within the box indicates mean.

neighbor. These "neighborless" tubulin subunits would be less stable in the lattice, as they are missing one lateral bond.

We simulated growth disruption of protofilaments by "targeting" random protofilament(s) (Fig. 4*A*, step 1). Here, "targeted" protofilament(s) would be entirely prevented from adding new tubulin subunits, thus preventing an increase in their length, for a specified amount of time (Fig. 4*A*, step 2). We then asked whether the targeting of protofilament(s) could ultimately destabilize the entire growing microtubule plus-end (Fig. 4*A*, step 3).

Prior to the start of each simulation, a random time point was selected for the targeting event to occur ($T_{targeted}$), and the number of protofilaments to be targeted was defined (Fig. 4*A*, step 1, $N_{targeted}$). A random protofilament was selected for targeting, and any additional targeted protofilaments were assigned to be adjacent to the initial selection, assuming that a single motor could potentially disrupt multiple adjacent protofilaments in a single curling event. Once the simulation started, tubulin subunits arrived, departed, and were stochastically hydrolyzed, up until the targeting event occurred. Once the targeting event occurred, growth was excluded from the targeted protofilament(s) for the duration of the targeting event (Fig. 4*A*, step 2, $D_{targeted}$) while stochastic hydrolysis continued. For the initial simulations, the targeting event lasted for 10 ± 1 s (mean ± SD), after which growth on the targeted protofilament(s) proceeded as normal. This assumption seemed reasonable, as the experimental Mal3–HSET interactions (in ATP) lasted for one to two time-lapse intervals at our sampling rate of 7.5 s per frame. Each simulation ran until a catastrophe event occurred, at which time, the simulation would end (Fig. 4*A*, step 3). The difference between the targeting event start time ($T_{targeted}$) and the catastrophe time at the end of the simulation was recorded for each simulation (Δt) as is shown in the representative simulation trace in Fig. 4*B* (Δt, green). To compare the simulation results to the experimental control results in which a random tip interaction time point was selected on microtubules with no motor tip interactions, a targeting start time was selected, but no protofilaments were selected for targeting (Fig. 4*C*, 0 protofilaments).

We first freely adjusted the tubulin concentration in the simulation in order to reproduce the control results in the HSET experiments (Fig. 4*C*, gray dash lines) and by targeting 0 protofilaments in the simulation (Fig. 4*C*, magenta). Then, we performed simulations in which we gradually increased the number of targeted protofilaments and plotted the average simulated time to catastrophe after the start of each targeting event (Fig. 4*C*, magenta, each data point represents a minimum of 100 simulations). Surprisingly, we found that the best fit between the HSET ATP experimental data (Fig. 4*C*, green lines) and the simulations (Fig. 4*C*, magenta) was when one protofilament was disrupted for ∼10 s. Thus, even a substoichiometric tip interaction for a brief period of time led to a substantial increase in the likelihood of catastrophe after the targeting event (Kinesin-14 motor(s) disrupting one protofilament of a 13-protofilament microtubule). We note that the disruption of two protofilaments for a shorter period of time (∼7 s) could also reproduce the experimentally observed time to catastrophe after an HSET tip interaction (*SI Appendix*, Fig. S3*A*).

Single Protofilament Disruption by Kinesin-14 Motors Is Consistent with Mal3 Fluorescence Signal Loss. Based on our simulations (Fig. 4 *A*–*C*), we predicted that the best fit to our experimental catastrophe data were if the Kinesin-14 motors disrupted approximately one to two protofilaments at the growing microtubule tip, perhaps by curling them away from the tip (Fig. 4*C*). Similarly, if the Kinesin-14 motors pulled Mal3 from the tips of one to two protofilaments, the loss in Mal3-mCherry fluorescence intensity after a Kinesin-14 tip interaction would be expected to be small.

Thus, we experimentally measured the Mal3-mCherry fluorescence in a 2 × 2–pixel box just prior to a Kinesin-14 tip interaction and then immediately following the tip interaction (Fig. 4 *D*, *Left*, white boxes). We found that the ratio of Mal3 fluorescence intensity after a Kinesin-14 tip interaction to the fluorescence intensity before the interaction was ∼94% (Fig. 4 *D*, *Right*). Thus, the experimental Mal3 fluorescence loss after a Kinesin-14 tip interaction is small, consistent with the simulation prediction that the Kinesin-14 motors may disrupt only a small fraction of protofilaments at the growing microtubule plus-end, although we note that rapid reassociation of EB proteins could also contribute to this effect.

We note that, when Mal3 and the Kinesin-14 motor(s) moved together away from a growing microtubule plus-end, this simultaneous movement was then defined as a tip pulling-away event (Fig. 4 *D*, *Left*, yellow dashed line), regardless of the degree of Mal3 signal change at the growing microtubule plus-end. Thus, in our model, we consider Mal3 to be a "handle" that is associated with protofilament(s) at the growing microtubule plus-end: when Kinesin-14 molecules bind to and pull on the Mal3 "handle," this may allow the Kinesin-14 molecules to exert minus-end–directed forces at the microtubule tip, thus disrupting the configuration and growth of the tip.

Generic Minus-End–Directed Forces at the Plus-End of Dynamic Microtubules Lead to Premature Catastrophe Events. To determine whether our Kinesin-14–EB findings were representative of a more general phenomenon in which minus-end–directed forces could alter the dynamics at growing microtubule plus-ends, we conducted DNA-tethering experiments (44). In these experiments, growing microtubule plus-ends were tethered to imaging coverslips using a DNA tether (Fig. 4*E*, green). The effect of the resultant minus-end–directed force on the likelihood of a catastrophe event was then measured (Fig. 4 *E*, *Right*). Specifically, we conjugated opposite complementary ends of λ-DNA with biotin or digoxigenin as previously described (45). Then, these ends were ligated together to form an 11-kb tether, and the final tether assembly was stained with a green YOYO1 label (44, 46). This allowed for the adhering of biotinylated yeast Dam1 complexes to one end of the tether. Purified Dam1 complexes have been previously shown to track the tips of dynamic microtubules (47–51) and make load-bearing attachments at dynamic microtubule ends (6, 52) (Fig. 4 *D*, *Right*). The opposite end of the tether, labeled with digoxigenin, was attached to coverslips prior to the start of the imaging experiment (Fig. 4*E*, blue).

Thus, as dynamic microtubules grew, their Dam1-bound plus-ends were caught and tethered by the DNA tethers (Fig. 4 *E*, *Right*). As the plus-ends continued to grow, this tether exerted a minus-end–directed force at the growing microtubule plus-end (Fig. 4 *E*, *Right*). TIRF imaging data were collected, and kymographs were constructed from videos of microtubules growing in the presence of tethers, with nontether binding microtubules used as controls.

In the DNA tether experiments, we observed dynamic microtubule plus-ends interacting with the green DNA–Dam1 tether assembly (Fig. 4*F*, white dashed arrow shows direction of microtubule growth; *SI Appendix*, Fig. S3*B* and Movie S5). Importantly, catastrophe events followed the interaction of growing plus-ends with the green tethers (Fig. 4*G*, yellow arrows). Any direct interaction of a growing microtubule plus-end with a green DNA tether was scored, and the total growth distance prior to catastrophe, past the nearest edge of the tether in the microtubule's direction of growth (Fig. 4*G*, white arrows), was measured. We then compared these tethered catastrophe distances to control catastrophe distances in which

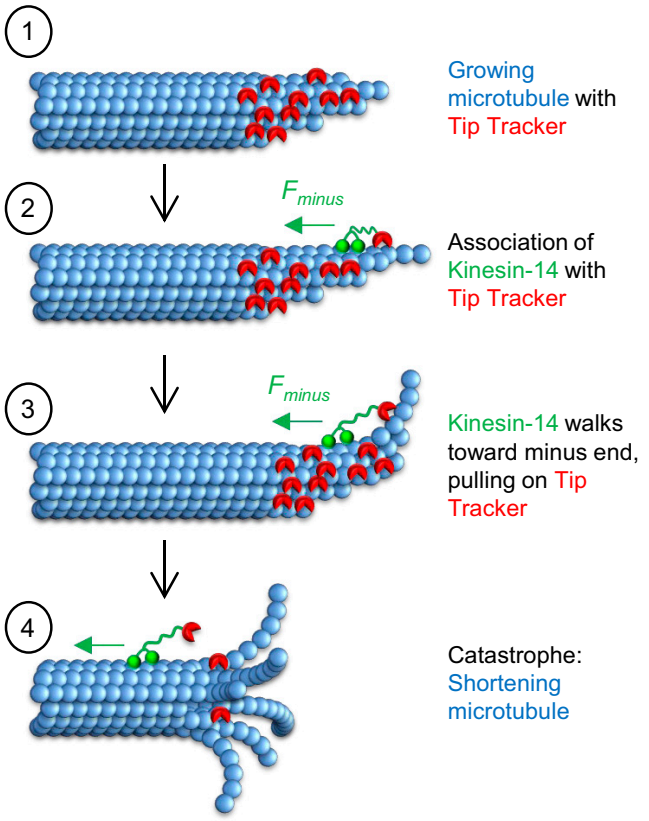

Fig. 5. The model for minus-end–directed regulation of microtubule dynamics via Kinesin-14 motors. The proposed mechanism by which minus-end–directed forces could result in a destabilization of the plus-end of growing microtubules, resulting in catastrophe. Step 1: EB tip tracker associates with protofilaments at the growing plus-end tip. Step 2: a Kinesin-14 motor binds to an EB tip tracker. Step 3: the Kinesin-14 motor begins walking toward the minus-end, exerting a minus-end–directed force (F_{minus}) on the EB tip tracker and, subsequently, on the protofilament(s) to which the EB protein is bound. This leads to disruption and/or curling of the protofilament(s). Step 4: the plus-end is destabilized, resulting in catastrophe.

a uniformly distributed random interaction point was selected on control microtubules that had no interactions with a DNA tether ("control interactions"; Movie S5; *Materials and Methods*). We found that the catastrophe distance was curtailed by approximately sevenfold after a tether interaction, relative to control (nontether) interactions (Fig. 4*H* and *SI Appendix*, Fig. S3*D*, $P < 0.0001$, K-S test).

By calculating the force required to stretch a DNA tether (*Materials and Methods*), we generated a plot of theoretical tether tension as a function of tether stretch distance (*SI Appendix*, Fig. S3*E*). Based on the distance that a plus-end grew past its DNA tether location prior to catastrophe (Fig. 4*E*, white arrows), we predict that, similar to HSET stall forces (21), the tether tension forces at catastrophe are small, likely <2 pN (*SI Appendix*, Fig. S3*E*).

Taken together, these results demonstrate that generic minus-end–directed forces exerted at growing microtubule plus-ends lead to premature catastrophe events, likely because of the disruption of protofilament growth.

Discussion

The dynamic growth and shrinkage of microtubules is a critical aspect of many cellular processes, including cell division and cellular trafficking of cargo. The improper regulation of microtubule dynamics within cells can have deleterious consequences. Thus, deciphering the mechanisms by which these processes are regulated is important not only for understanding normal cellular processes but can also help in the understanding of disease states. The close relationship between microtubules and the Kinesin-14 motor proteins that move along them has been well established to be important in cell division (9). We now show that Kinesin-14 motor proteins participate in a regulatory force–balance interaction at the plus-ends of growing microtubules. By exerting minus-end–directed forces at growing microtubule plus-ends, the interaction of Kinesin-14 motors with EB tip trackers leads to the increased likelihood of catastrophe events.

We found that, in the presence of EB proteins, Kinesin-14 motors can associate with growing microtubule plus-ends before walking toward the minus-end (Fig. 5, steps 1 to 2). Notably, minus-end–directed Kinesin-14 motor forces pull EB proteins off of the growing microtubule tip (Fig. 5, step 3), leading to an increased likelihood of premature catastrophe (Fig. 5, step 4). Specifically, by binding EB proteins and pulling them away from the growing microtubule tip, Kinesin-14 motors may remove tubulin subunits and/or pull back on protofilaments at the growing microtubule end (Fig. 5, step 3), causing catastrophe (Fig. 5, step 4). Consistent with this model, we found that, in cells, both individual astral microtubules and bundles of anaphase interpolar microtubules were longer when the interaction of Kinesin-14 motors with EB proteins was disrupted (Fig. 1). Our results are consistent with a recent report that demonstrated increased dendritic microtubule bundle elongation in the absence of the Kinesin-14 motor KIFC3 (22). Furthermore, Kar3/Cik1 Kinesin-14 motors have been shown to block microtubule nucleation in yeast and in human cell lines (17, 53), suggesting that minus-end–directed Kinesin-14 motors could exert forces to frustrate microtubule plus-end growth.

It has been shown that HSET and free tubulin form heterogeneous clusters in solution and that this clustering behavior increases the processivity of the HSET motor on dynamic microtubules (18). Consistent with these results, we found that, in the presence of free tubulin, HSET moves processively along the dynamic microtubule lattice, regardless of whether or not it carried an EB protein along with it (Fig. 2). Importantly, heterogeneous clustering of HSET with free tubulin would allow multiple EB molecules to be bound during HSET–EB tip interactions, potentially pulling multiple EB molecules along and thus more dramatically disrupting the plus-end structure as HSET walks away from the tip.

Based on our simulation and DNA-tethering results, we conclude that a force balance between growing microtubule plus-ends and minus-end–directed motor forces can act to regulate microtubule dynamics. Specifically, by pulling EB proteins from growing microtubule plus-ends, Kinesin-14 motors proteins could curl back or disrupt protofilaments at the microtubule plus-end, thus frustrating their coordinated growth with the remainder of the protofilaments. Our simulations predict that an ~7- to 10-s disruption of one to two protofilaments could reproduce our experimental results, indicating that brief interactions with rapidly turning over EB proteins are sufficient to destabilize the growing microtubule plus-end.

We do not expect that the loss of Mal3 from the growing microtubule end in itself is responsible for a catastrophe event, as 1) the fractional loss of Mal3 from the growing microtubule plus-end after a Kinesin-14 interaction event is small (Fig. 4*D*), 2) Mal3/EB1 at the growing microtubule end is not thought to stabilize plus-end growth but rather to increase the likelihood of catastrophe events at growing microtubule ends by accelerating the hydrolysis rate of GTP-tubulin at the tip of the microtubule (54), and 3) new Mal3 molecules could reassociate quickly with the growing microtubule tip after a tip removal event.

However, while the loss of EB proteins at the growing microtubule tip seems unlikely to explain our results, alternative biophysical explanations for our results are possible. For example, the motor-EB complex could act to remove tubulin subunits from the growing microtubule plus-end, thus exposing GDP-tubulin subunits and instigating a catastrophe event, analogous to the "bump off" model for tubulin dimer removal by the plus-end–directed Kinesin-8 motor Kip3 (55).

A recent in vitro study found that Kinesin-14 motors act to stabilize the microtubule minus-end by suppressing the tubulin off rate (19). Strikingly, we found that, when minus-end–directed mobility was impaired, the Kinesin-14 motors tracked and similarly stabilized growing microtubule plus-ends. Thus, we conclude that the ability of Kinesin-14 motors to destabilize growing microtubule plus-ends depends on their ability to generate minus-end–directed forces at the growing microtubule tip. The force required to bend or curl a single microtubule protofilament is likely ∼1.25 pN (56, 57), and moving HSET motors have been shown to exert ∼1 to 2 pN of tension force (21). Thus, while the force exerted by Kinesin-14 motors on the tubulin subunits and EB proteins at the plus-end tip may be weak and transient, our evidence suggests that minus-end–directed forces are an important component to regulating microtubule plus-end growth and catastrophe.

We found that Kinesin-14 motors with inhibited minus-end motility are guided along in a plus-end direction by associating with Mal3 proteins at the plus-end of growing microtubules (Fig. 3). In this case, the EB tip tracker "wins" the force balance competition, leading to the opposite effect of the force-generating motor: plus-end growth is stabilized by motility-inhibited Kinesin-14 motors that are pulled along with the growing plus-end. This behavior may be due to a mobility-inhibited but not strongly bound motor or by a second microtubule binding domain on the HSET N-terminal tail domain, both of which could contribute to persistent binding to and diffusive-like transport on microtubules (21). In this way, the tail binding of HSET to microtubules would allow HSET to track the growing microtubule plus-end, regardless of rapid individual EB protein turnover (58–60), as the HSET molecules could rapidly "trade off" EB binding partners. Alternatively, because Kinesin-14 tails bind to the microtubule lattice independently of EB proteins, Kinesin-14 motors could trap individual EB proteins near to the microtubule tip via tail binding, increasing their likelihood of rebinding to protofilaments at the growing microtubule tip.

Similar to our results in AMP-PNP, it has been previously shown that Kinesin-14 motors can reverse direction and thus be pulled along by EB1 at growing microtubule plus-ends to guide the growth of parallel microtubules from mating projections in budding yeast (26). In this work by Molodtsov et al., the authors found that Kar3/Cik1 tracked with Mal3 at growing microtubule plus-ends, similar to our AMP-PNP results for HSET. In contrast, we found that Kar3/Cik1 pulled Mal3 proteins away from the growing microtubule plus-end and then traveled processively toward the minus-end. We suspect that the difference in our results was in the phosphorylation state of the Kar3/Cik1 motor: we purified Kar3/Cik1 directly from yeast cells in log phase in the presence of phosphatase inhibitors, and so the motors are in a native mitotic phosphorylation state. In contrast, Molodtsov et al. purified Kar3/Cik1 from SF9 insect cells, and thus, the motors were likely dephosphorylated. Interestingly, Molodtsov et al. found that Cdc28/Cdk1-phosphorylated Kar3/Cik1 no longer tracked diffusively with Mal3 at the plus-end tip but rather moved processively in the minus-end direction on the microtubule lattice, consistent with our results using mitotic yeast purified Kar3/CIk1 protein. Thus, it seems likely that the phosphorylation state of Kar3/Cik1 dictates its mobility and/or its interaction with Mal3 and therefore its ability to regulate microtubule plus-end dynamics, especially during mitosis. Furthermore, we note that differences in the phosphorylation state of the EB protein itself could also regulate its interaction with Kinesin-14 motors (61).

We note that Molodtsov et al. observed tip tracking of HSET with EB1 at growing plus-ends under higher salt conditions (100 mM KCl) (26). We tested our HSET/Mal3 assay at 100 mM KCl, and while interactions of Kinesin-14 with the microtubule lattice were much less frequent than in our lower salt experiments (55 mM KCl), we still occasionally observed Kinesin-14 molecules pulling Mal3 away from the growing plus-end (*SI Appendix*, Fig. S3*C*). In earlier work, Braun et al. performed similar experiments but under even higher salt conditions (150 mM KCl) (62). Here, the authors exclusively observed tip tracking of HSET–GFP in the presence of unlabeled EB1 and did not observe interactions of Kinesin-14 with the microtubule lattice (62). Thus, a higher salt concentration may cause HSET–GFP to bind preferentially to EB1 rather than to the microtubule lattice. Consistent with this idea, we observed processive HSET–GFP lattice interactions in the presence of EB1–GFP at lower salt concentrations (*SI Appendix*, Fig. S2*C*, 55 mM KCl). Regardless, our results with HSET in AMP-PNP are consistent with the previously described ability of Kinesin-14 motors to move in both plus-end and minus-end directions for microns when unloaded (21, 26).

In summary, our work illustrates the diversity of function for force-generating kinesin motors in both regulating microtubule dynamics and in transporting cargo along microtubule tracks within the cell. While previous work implicates Kinesin-8 molecular motors in pushing tubulin subunits from the ends of growing microtubules to disrupt growth and promote catastrophe events (55, 63), we now describe an opposite role for Kinesin-14 motors in pulling EB proteins from growing microtubule ends to disrupt growth and promote catastrophe events. Interesting future work will explore the single-molecule nanoscale mechanisms to explain how EB removal from growing microtubule plus-ends leads to rapid catastrophe events.

Materials and Methods

Detailed materials and methods are included in expanded *SI Appendix, SI Materials and Methods*.

Tubulin and protein purifications were completed as described in *SI Appendix, SI Materials and Methods*. Stable GMPCPP seed templates were assembled, which were then adhered in flow chambers that were assembled for TIRF microscopy. For the dynamic microtubule assays, a reaction mixture including imaging buffer to reduce photobleaching was made according to detailed *SI Appendix, SI Materials and Methods*. For motor experiments, 2 nM Kar3-GFP/Cik1or Kar3-GFP/Cik1-4A or 1 nM HSET–GFP was included in the reaction mixture. For the cell experiments, *Saccharomyces cerevisiae* yeast strains used in the study were per *SI Appendix*, Table S1, with culture and imaging conditions as described in *SI Appendix, SI Materials and Methods*.

The quantitative analysis of midzone length and astral microtubule lengths in cells was completed using ImageJ and MATLAB as described in supplemental methods. Kymographs for each dynamic microtubule extension were generated and analyzed using ImageJ. For the control data, control microtubules were selected from the kymographs with no motor interaction during the entire growth cycle. The total microtubule growth time prior to catastrophe ("catastrophe time") was measured for each control microtubule, and then each catastrophe time was multiplied by a uniformly distributed random number between 0 and 1 to generate a theoretical tip interaction time point. The difference between this theoretical tip interaction time point and its associated control microtubule catastrophe time represented the values for the control data set in each dynamic microtubule experiment. For the AMP-PNP experiments, the tip interaction time was defined as the total time during which any green fluorescence above background (Kinesin-14 motor fluorescence) occupied the same pixel as the extreme microtubule plus-end tip fluorescence.

Computational simulations were completed in MATLAB as described in *SI Appendix, SI Materials and Methods*.

Data Availability. All study data are included in the article and/or supporting information.

ACKNOWLEDGMENTS. The Gardner Laboratory is supported by NIH National Institute of General Medical Sciences (NIGMS) Grant R35-GM126974. E.D. was supported by NIGMS Grant R01 GM040506 to T.N.D. A.O. was supported by NIH NIGMS Training Program in Muscle Research Grant T32AR007612.We thank members of the Gardner Laboratory for helpful discussions. We thank Dr. Thomas Surrey for the generous gift of Mal3 constructs and Dr. Marija Zanic for the generous gift of HSET–GFP constructs.

1. A. Desai, T. J. Mitchison, Microtubule polymerization dynamics. *Annu. Rev. Cell Dev. Biol.* **13**, 83–117 (1997).
2. T. Mitchison, M. Kirschner, Dynamic instability of microtubule growth. *Nature* **312**, 237–242 (1984).
3. M. K. Gardner, M. Zanic, J. Howard, Microtubule catastrophe and rescue. *Curr. Opin. Cell Biol.* **25**, 14–22 (2013).
4. M. E. Janson, M. E. de Dood, M. Dogterom, Dynamic instability of microtubules is regulated by force. *J. Cell Biol.* **161**, 1029–1034 (2003).
5. A. G. Hendricks *et al.*, Dynein tethers and stabilizes dynamic microtubule plus ends. *Curr. Biol.* **22**, 632–637 (2012).
6. A. D. Franck *et al.*, Tension applied through the Dam1 complex promotes microtubule elongation providing a direct mechanism for length control in mitosis. *Nat. Cell Biol.* **9**, 832–837 (2007).
7. K. Jaqaman *et al.*, Kinetochore alignment within the metaphase plate is regulated by centromere stiffness and microtubule depolymerases. *J. Cell Biol.* **188**, 665–679 (2010).
8. B. Akiyoshi *et al.*, Tension directly stabilizes reconstituted kinetochore-microtubule attachments. *Nature* **468**, 576–579 (2010).
9. Z. Y. She, W. X. Yang, Molecular mechanisms of kinesin-14 motors in spindle assembly and chromosome segregation. *J. Cell Sci.* **130**, 2097–2110 (2017).
10. A. Mitra *et al.*, Kinesin-14 motors drive a right-handed helical motion of antiparallel microtubules around each other. *Nat. Commun.* **11**, 2565 (2020).
11. A. J. Hepperla *et al.*, Minus-end-directed Kinesin-14 motors align antiparallel microtubules to control metaphase spindle length. *Dev. Cell* **31**, 61–72 (2014).
12. L. Winters *et al.*, Pivoting of microtubules driven by minus-end-directed motors leads to spindle assembly. *BMC Biol.* **17**, 42 (2019).
13. S. Cai, L. N. Weaver, S. C. Ems-McClung, C. E. Walczak, Kinesin-14 family proteins HSET/XCTK2 control spindle length by cross-linking and sliding microtubules. *Mol. Biol. Cell* **20**, 1348–1359 (2009).
14. G. Goshima, J. M. Scholey, Control of mitotic spindle length. *Annu. Rev. Cell Dev. Biol.* **26**, 21–57 (2010).
15. G. Goshima, R. Wollman, N. Stuurman, J. M. Scholey, R. D. Vale, Length control of the metaphase spindle. *Curr. Biol.* **15**, 1979–1988 (2005).
16. G. Goshima, F. Nédélec, R. D. Vale, Mechanisms for focusing mitotic spindle poles by minus end-directed motor proteins. *J. Cell Biol.* **171**, 229–240 (2005).
17. B. R. King *et al.*, Microtubule-associated proteins and motors required for ectopic microtubule array formation in *Saccharomyces cerevisiae*. *Genetics* **218**, iyab050 (2021).
18. S. R. Norris *et al.*, Microtubule minus-end aster organization is driven by processive HSET-tubulin clusters. *Nat. Commun.* **9**, 2659 (2018).
19. C. Strothman *et al.*, Microtubule minus-end stability is dictated by the tubulin off-rate. *J. Cell Biol.* **218**, 2841–2853 (2019).
20. C. Mieck *et al.*, Non-catalytic motor domains enable processive movement and functional diversification of the kinesin-14 Kar3. *eLife* **4**, e04489 (2015).
21. D. N. Reinemann, S. R. Norris, R. Ohi, M. J. Lang, Processive kinesin-14 HSET exhibits directional flexibility depending on motor traffic. *Curr. Biol.* **28**, 2356–2362.e5 (2018).
22. Y. Cao *et al.*, Microtubule minus-end binding protein CAMSAP2 and kinesin-14 motor KIFC3 control dendritic microtubule organization. *Curr. Biol.* **30**, 899–908.e6 (2020).
23. S. A. Endow *et al.*, Yeast Kar3 is a minus-end microtubule motor protein that destabilizes microtubules preferentially at the minus ends. *EMBO J.* **13**, 2708–2713 (1994).
24. S. Honnappa *et al.*, An EB1-binding motif acts as a microtubule tip localization signal. *Cell* **138**, 366–376 (2009).
25. N. Kornakov, B. Möllers, S. Westermann, The EB1-Kinesin-14 complex is required for efficient metaphase spindle assembly and kinetochore bi-orientation. *J. Cell Biol.* **219**, e202003072 (2020).
26. M. I. Molodtsov *et al.*, A force-induced directional switch of a molecular motor enables parallel microtubule bundle formation. *Cell* **167**, 539–552.e14 (2016).
27. E. Szczęsna, A. A. Kasprzak, Insights into the process of EB1-dependent tip-tracking of kinesin-14 Ncd. The role of the microtubule. *Eur. J. Cell Biol.* **95**, 521–530 (2016).
28. S. P. Maurer, P. Bieling, J. Cope, A. Hoenger, T. Surrey, GTPgammaS microtubules mimic the growing microtubule end structure recognized by end-binding proteins (EBs). *Proc. Natl. Acad. Sci. U.S.A.* **108**, 3988–3993 (2011).
29. I. Brust-Mascher, G. Civelekoglu-Scholey, M. Kwon, A. Mogilner, J. M. Scholey, Model for anaphase B: Role of three mitotic motors in a switch from poleward flux to spindle elongation. *Proc. Natl. Acad. Sci. U.S.A.* **101**, 15938–15943 (2004).
30. M. K. Gardner *et al.*, The microtubule-based motor Kar3 and plus end-binding protein Bim1 provide structural support for the anaphase spindle. *J. Cell Biol.* **180**, 91–100 (2008).
31. R. B. Nicklas, Measurements of the force produced by the mitotic spindle in anaphase. *J. Cell Biol.* **97**, 542–548 (1983).
32. D. Pellman, M. Bagget, Y. H. Tu, G. R. Fink, H. Tu, Two microtubule-associated proteins required for anaphase spindle movement in *Saccharomyces cerevisiae*. *J. Cell Biol.* **130**, 1373–1385 (1995).
33. G. C. Rogers *et al.*, Two mitotic kinesins cooperate to drive sister chromatid separation during anaphase. *Nature* **427**, 364–370 (2004).
34. A. F. Straight, J. W. Sedat, A. W. Murray, Time-lapse microscopy reveals unique roles for kinesins during anaphase in budding yeast. *J. Cell Biol.* **143**, 687–694 (1998).
35. R. Subramanian, J. Gelles, Two distinct modes of processive kinesin movement in mixtures of ATP and AMP-PNP. *J. Gen. Physiol.* **130**, 445–455 (2007).
36. S. A. Cohn, A. L. Ingold, J. M. Scholey, Quantitative analysis of sea urchin egg kinesin-driven microtubule motility. *J. Biol. Chem.* **264**, 4290–4297 (1989).
37. N. R. Guydosh, S. M. Block, Backsteps induced by nucleotide analogs suggest the front head of kinesin is gated by strain. *Proc. Natl. Acad. Sci. U.S.A.* **103**, 8054–8059 (2006).
38. S. W. Manka, C. A. Moores, Microtubule structure by cryo-EM: Snapshots of dynamic instability. *Essays Biochem.* **62**, 737–751 (2018).
39. R. Ayukawa *et al.*, GTP-dependent formation of straight tubulin oligomers leads to microtubule nucleation. *J. Cell Biol.* **220**, e202007033 (2021).
40. S. W. Manka, C. A. Moores, The role of tubulin-tubulin lattice contacts in the mechanism of microtubule dynamic instability. *Nat. Struct. Mol. Biol.* **25**, 607–615 (2018).
41. C. E. Coombes, A. Yamamoto, M. R. Kenzie, D. J. Odde, M. K. Gardner, Evolving tip structures can explain age-dependent microtubule catastrophe. *Curr. Biol.* **14**, 1342–1348 (2013).
42. H. T. Schek III, M. K. Gardner, J. Cheng, D. J. Odde, A. J. Hunt, Microtubule assembly dynamics at the nanoscale. *Curr. Biol.* **17**, 1445–1455 (2007).
43. V. VanBuren, L. Cassimeris, D. J. Odde, Mechanochemical model of microtubule structure and self-assembly kinetics. *Biophys. J.* **89**, 2911–2926 (2005).
44. S. Diez *et al.*, Stretching and transporting DNA molecules using motor proteins. *Nano Lett.* **3**, 1251–1254 (2003).
45. R. Yokokawa, J. Miwa, M. C. Tarhan, H. Fujita, M. Kasahara, DNA molecule manipulation by motor proteins for analysis at the single-molecule level. *Anal. Bioanal. Chem.* **391**, 2735–2743 (2008).
46. C. Z. Dinu *et al.*, Parallel manipulation of bifunctional DNA molecules on structured surfaces using kinesin-driven microtubules. *Small* **2**, 1090–1098 (2006).
47. J. F. Tien *et al.*, Cooperation of the Dam1 and Ndc80 kinetochore complexes enhances microtubule coupling and is regulated by aurora B. *J. Cell Biol.* **189**, 713–723 (2010).
48. F. Lampert, P. Hornung, S. Westermann, The Dam1 complex confers microtubule plus end-tracking activity to the Ndc80 kinetochore complex. *J. Cell Biol.* **189**, 641–649 (2010).
49. C. L. Asbury, D. R. Gestaut, A. F. Powers, A. D. Franck, T. N. Davis, The Dam1 kinetochore complex harnesses microtubule dynamics to produce force and movement. *Proc. Natl. Acad. Sci. U.S.A.* **103**, 9873–9878 (2006).
50. S. Westermann *et al.*, The Dam1 kinetochore ring complex moves processively on depolymerizing microtubule ends. *Nature* **440**, 565–569 (2006).
51. D. R. Gestaut *et al.*, Phosphoregulation and depolymerization-driven movement of the Dam1 complex do not require ring formation. *Nat. Cell Biol.* **10**, 407–414 (2008).
52. V. A. Volkov *et al.*, Long tethers provide high-force coupling of the Dam1 ring to shortening microtubules. *Proc. Natl. Acad. Sci. U.S.A.* **110**, 7708–7713 (2013).
53. Z. T. Olmsted, A. G. Colliver, T. D. Riehlman, J. L. Paluh, Kinesin-14 and kinesin-5 antagonistically regulate microtubule nucleation by γ-TuRC in yeast and human cells. *Nat. Commun.* **5**, 5339 (2014).
54. R. Zhang, B. LaFrance, E. Nogales, Separating the effects of nucleotide and EB binding on microtubule structure. *Proc. Natl. Acad. Sci. U.S.A.* **115**, E6191–E6200 (2018).
55. V. Varga, C. Leduc, V. Bormuth, S. Diez, J. Howard, Kinesin-8 motors act cooperatively to mediate length-dependent microtubule depolymerization. *Cell* **138**, 1174–1183 (2009).
56. E. L. Grishchuk *et al.*, The Dam1 ring binds microtubules strongly enough to be a processive as well as energy-efficient coupler for chromosome motion. *Proc. Natl. Acad. Sci. U.S.A.* **105**, 15423–15428 (2008).
57. H. W. Wang, E. Nogales, Nucleotide-dependent bending flexibility of tubulin regulates microtubule assembly. *Nature* **435**, 911–915 (2005).
58. P. Bieling *et al.*, CLIP-170 tracks growing microtubule ends by dynamically recognizing composite EB1/tubulin-binding sites. *J. Cell Biol.* **183**, 1223–1233 (2008).
59. P. Bieling *et al.*, Reconstitution of a microtubule plus-end tracking system in vitro. *Nature* **450**, 1100–1105 (2007).
60. K. E. Busch, J. Hayles, P. Nurse, D. Brunner, Tea2p kinesin is involved in spatial microtubule organization by transporting tip1p on microtubules. *Dev. Cell* **6**, 831–843 (2004).
61. Y. Song *et al.*, The microtubule end-binding affinity of EB1 is enhanced by a dimeric organization that is susceptible to phosphorylation. *J. Cell Sci.* **133**, jcs241216 (2020).
62. M. Braun *et al.*, The human kinesin-14 HSET tracks the tips of growing microtubules in vitro. *Cytoskeleton (Hoboken)* **70**, 515–521 (2013).
63. V. Varga *et al.*, Yeast kinesin-8 depolymerizes microtubules in a length-dependent manner. *Nat. Cell Biol.* **8**, 957–962 (2006).